

A BEAM MONITOR SYSTEM FOR HIGH-INTENSITY PHOTON BEAMS  
IN THE MULTI-BEV RANGE\*

G. E. Fischer and Y. Murata†  
Stanford Linear Accelerator Center  
Stanford University, Stanford, California 94305

ABSTRACT

A system of instruments used to monitor the high-power SLAC photon beam is described. Operational experience in a series of photoproduction experiments shows an overall accuracy of  $\pm 1\%$  with beam powers from 100 watts to 3.5 kW at bremsstrahlung end point energies from 5 to 18 GeV.

(Submitted to Nucl. Instr. and Methods.)

---

\*Work supported by the U.S. Atomic Energy Commission.

†On leave from the Institute for Nuclear Study, University of Tokyo, Japan.

## I. INTRODUCTION

We present here the details of a photon beam monitor system whose properties arise partly from the characteristics of the SLAC accelerator beam and partly from the apparatus used in a series of experiments designed to study meson photoproduction in the multi-GeV range.<sup>1</sup> We believe that although no new concepts are introduced, this work is of interest because otherwise well-known instruments are modified and used together in new ways.

The bremsstrahlung photon beam at End Station A at SLAC (see Fig. 1) is produced by a high-power momentum-analyzed electron beam striking an aluminum radiator typically 0.03 radiation length thick. After passing through the radiator, the electron beam is bent downward into a water-cooled dump capable of absorbing up to 300 kilowatts of power. The bremsstrahlung beam is collimated to reduce the transverse size of the photon beam at the particle production target located about 50 m downstream from the radiator. The size of the beam at the production target is dictated by the requirements of a particular experiment. In our experiments this size is normally  $1 \times 3$  cm vertically and horizontally. The monitoring problem is, therefore, to measure with an accuracy of about 1% the intensity of a photon beam of average power between a few tens of watts and 3 kilowatts, which arrives at the target in  $1.5 \mu$  sec-long bursts, usually at repetition rates of about 180 pps.

There are basically three different types of photon monitors each in its way sensitive to a different part of the spectrum. With a pair spectrometer for instance one can examine in detail the shape of the spectrum near its end point. A total energy monitor measures the power of the beam integrated over all energies. Thin ion chambers or thin secondary emission monitors are sensitive

to the total number of photons and their response is therefore dominated by low energy photons.

Since the experiments of interest to us are performed with the high-energy tip of the spectrum, logically the pair spectrometer method would be most applicable were it not for duty cycle problems and geometrical restrictions inherent in the set up of the apparatus. Thin monitors of the type mentioned above not only measure the wrong part of the spectrum but are terribly sensitive to contamination caused by the collimators in spite of the fact that sweeping magnets are used to clear charged particles out of the beam. We have therefore concentrated our attention on total energy monitors even though they will necessarily destroy the beam. The relevant number of photons is computed from total energy by a thick target bremsstrahlung calculation<sup>2</sup> suitably corrected for collimation effects.<sup>3</sup>

It is clear that gas-filled quantimeters,<sup>4</sup> standard instruments at circular electron accelerators, would be saturated at the power densities mentioned above. The high power of the beam leads one at once to calorimetry, but two special requirements are placed on the design of the instrument by the experiments in which it is to be used. First, the high data rate inherent in these experiments, which is handled by a computer, requires that monitor data be processed with a minimum delay — in some runs the momentum setting of the spectrometer is stepped every 15 sec. Second, because photoproduction reactions are interesting at very small momentum transfer, that is at very small forward angles, severe restrictions are placed on the physical size of the monitor to avoid its intrusion into the acceptance of the spectrometer. These considerations led us to what we call a MINISEQ — a very small modified secondary emission quantimeter<sup>5</sup> for use as the non-saturating operational monitor (see Fig. 2). In some ways, this

instrument resembles in operation a gasless thick-walled ionization chamber.<sup>6</sup> This small device, not capable of absorbing the total shower energy completely, must be calibrated and checked periodically to insure that the secondary emission coefficient of the foils have not changed with either time or radiation density.

Absolute calibrations of the MINISEQ are carried out against two calorimeters,<sup>7,8</sup> one of them high power, somewhat clumsy, large and made of copper; the other small with a short time constant, made of silver. They are shown in Fig. 3. The heat capacities of these devices are measured by using internal heaters and applying small corrections for photon capture efficiency obtained from Monte Carlo calculations.<sup>9</sup> An independent experimental check on the calorimeters is also provided by using an incident electron beam of accurately known energy<sup>10</sup> and total charge, measured by either the SLAC precision integrating toroid<sup>11</sup> or Faraday cup.<sup>12</sup>

The intercalibration of the MINISEQ with a calorimeter, both of which destroy the beam, requires a nondestructive photon beam monitor as a "transfer" standard. Further, at photoproduction angles very close to zero, even the MINISEQ is too large and must be removed from the beam. We have designed for these purposes a 1-meter-long helium gas Cerenkov counter<sup>13</sup> (see Fig. 4) which in this case measures the number of photons converted to electrons in its very thin aluminum entrance window. The virtue of the Cerenkov monitor, aside from being very thin, is that the threshold energy for electrons, when the counter is operated at 1 atmosphere of helium, is 60 MeV. This property makes the monitor much less sensitive to low-energy spray from the collimators than an ion chamber, for example.

Two other thin monitors — a multi-plate hydrogen-filled ion chamber and an oscillating secondary emission monitor (SEM) not described in this paper — are also placed in the beam just downstream of the Cerenkov monitor. Their use is primarily diagnostic. The ion chamber has horizontally and vertically split

sections built into it that serve to monitor the position of the photon beam and activate alarms.

In practice, during an experiment, before and after each data run the amounts of collected charge from the Cerenkov monitor, the SEM, and two outputs from a MINISEQ are read via vibrating reed-type feedback electrometer<sup>14</sup> integrators or an integrating digital voltmeter into the same computer which is used to collect the data from the particle detection apparatus. The primary electron beam is monitored by an integrating beam current transformer. A subroutine with appropriate calibration constants computes the cumulative number of equivalent quanta for each instrument and provides a monitor correlation matrix on line.

## II. CALORIMETERS

### A. Design

It was the original intent to build a calorimeter accurate enough to provide an independent absolute check on the SLAC beam switchyard energy. This use requires that the device must be large enough to capture enough of the electron cascade shower so that errors introduced by loss corrections would be very small. For the "laboratory standard," therefore, a copper cylinder 10 inches in diameter and 20 inches long was chosen, having 0.13% forward and lateral photon loss at 10 GeV.<sup>9</sup> Backscattering losses leaving the entrance face and energy loss by neutrons are estimated to be 0.012%<sup>9</sup> and 0.17%<sup>15</sup> respectively. Loss by  $\mu$ -meson pair production is negligible. Copper is superior to lead in that it will not melt at the anticipated power levels (up to 5 kW) and has good thermal conductivity. However, it was recognized early that the characteristic time to come to thermal equilibrium of a cylinder in which heat is deposited along its axis varies as  $a^2/\alpha$ , where  $a$  is the radius and  $\alpha$  the thermal diffusivity

$K/\rho C_V$ . In this relation  $K$  is the thermal conductivity,  $\rho$  the density and  $C_V$  the specific heat. By going to a material of higher thermal diffusivity and by reducing the radius thereby accepting a larger photon loss, the time constant could be appreciably lowered. Accordingly, a second calorimeter, having as a core a silver cylinder 12.5 cm in diameter and 21 cm long, was designed.

We now turn to a discussion of the calculation of the energy loss from these calorimeters. It has been found that the experimental data<sup>16</sup> on the lateral distribution of the energy deposition agree quite well with the Monte Carlo results, independent of choice of absorber material and incident energy, if the radial distance is measured in the Moliere unit " $r_m$ " defined by the equation

$$"r_m" = \frac{E_s}{\mathcal{E}_0} X_0$$

where  $E_s$  is a characteristic energy = 21.2 MeV,  
 $\mathcal{E}_0$  is the critical energy of the material,  
 $X_0$  is the radiation length of the material.

Further, Nagel and Völkel have showed for two kinds of material namely lead and copper, that if the longitudinal depth of the absorber is given in a form of  $t/\ln E_0$  (MeV) radiation length, the distribution of energy deposition does not depend critically on the primary energy  $E_0$ . According to analytic shower theory<sup>17</sup> the longitudinal development of the shower is described independently of absorber material and type of incident beam as well, by using the variable  $s$ , the so-called "shower age" as a measure of depth.  $s$  and  $t$  are related by the following equation

$$t = \frac{1}{\lambda'(s)} \left[ \ln \frac{E_0}{\mathcal{E}_0} - \frac{n}{s} \right]$$

in which  $n = 0.5$  for monochromatic photon-induced showers,  
 $= 1.0$  for electron-induced showers,  
 $= 1.5$  for bremsstrahlung photon-induced showers,  
and  $\lambda'(s)$  is a complicated function.<sup>17</sup>

In Fig. 5 we show a universal curve for the percentage energy loss  $F(s)$ , which was taken from the Monte Carlo calculations for 3 and 6 GeV, as a function of shower age for cylinders of radii 4.1 and 8.54 Molière units which correspond to the dimensions of the silver and copper calorimeters respectively. Assuming that the outlined procedure is correct, one may calculate the efficiency of the small silver calorimeter which is shown in Fig. 6. In general, calculating the relationship between  $s$  and  $t$  is quite tedious. Fortunately in the region of interest, where the percentage loss is small,  $\lambda'(s)$  may be approximated by  $-s^{-2}$ . If

$$\ln \left( \frac{E_0}{\mathcal{E}_0} \right) \gg \frac{n}{2} ,$$

the case for high-energy showers,  $s$  may be closely approximated by

$$s \approx \left[ \frac{t}{\ln \left( \frac{E_0}{\mathcal{E}_0} \right) - \frac{n}{2}} \right]^{1/2}$$

The energy loss shown in Fig. 6 does not include backscatter nor neutron losses.

#### B. Construction

Figure 3 shows how the metal cylinders of the calorimeters are mounted and insulated by blocks of light, rigid polyurethane foam. This material has a compression strength of 15 psi and a thermal conductivity of 0.25 BTU/hr/ft<sup>2</sup>/°F/in. Thermal radiation shields are provided by layers of aluminum-coated mylar,

spaced about 1 cm apart.\* For the large calorimeter, the water-cooling channels and heater well are drilled out of an ingot of OFHC copper. The smaller calorimeter was constructed by casting silver into a pre-heated mold in which the heater rod<sup>18</sup> and a helical thin-walled stainless steel tube were mounted. The heaters are located off-center in the front of the blocks to simulate as much as possible the heat source of the developing shower. Precision platinum resistance thermometers<sup>19</sup> are used so that no long-term calibration error due to radiation damage results.<sup>20</sup> The thermometer wells are placed in the rear of the blocks and at large radius so that the transient response to the heat pulse will not have an overshoot. As is the case for the MINISEQ, for rapid insertion into the beam, these instruments are mounted on a chain-driven cart that runs on rails just ahead of the spectrometer. Remotely-operated water valves permit the calorimeters to be cooled rapidly. Cooling water is blown out of the coils with air after each use, to make certain the thermal mass of the devices remains constant and to reduce heat leaks. A diagram of the electrical instrumentation is shown in Fig. 7. The voltage across the resistance of the thermometers is read directly into the integrating digital voltmeter, which forms the heart of the system. This instrument also monitors the thermometer reference current and can measure the dc input current and voltage to the heaters. (The integrating feature of the digital voltmeter provides excellent common mode rejection on the thermometer leads resulting in noise figures of a few microvolts.) These parameters are printed in digital form every few seconds, as either measurement or calibration proceeds. The precise electric heating time may be read to a tenth of a second from a clock.

---

\* In a newer version, an electrically-heated thermal guard ring is employed.

### C. Operation

Figure 8 shows a typical response to electrical and electron beam calibration runs. During the heating time the resistance of the heaters changes slightly so that the evaluation of  $J = \int_0^t VI dt$  is performed by numerical integration. If the thermometer current is adjusted to 1 milliamp by adjusting the voltage across the 100 ohm reference resistor to exactly 100 millivolts, the reduction of the thermometer millivolt readings to heat input, J, is performed by the relation,

$$J = \Delta H = C(T_{av})(T_2 - T_1) = \frac{mv_2 - mv_1}{\alpha_J C'}$$

where  $C(T_{av})$  is the thermal capacity of the calorimeter at average temperature

$$T_{av},$$

$C'$  is the calorimeter calibration constant independent of  $T_{av}$ ,

$T_2 - T_1$  is the rise in temperature in degrees centigrade,

$mv_1$  and  $mv_2$  are the cold and warm millivolt readings at thermal equilibrium,

and  $\alpha_J$  is an effective conversion "constant" that corrects for the nonlinear thermometer response and the variation of specific heat of the metal with average temperature (see Fig. 9).

If the electrical calibration is carried out at the same power level, average temperature above ambient and time as during an electron or photon beam run, no cooling correction need be applied and a direct intercalibration ratio may be taken. Even so, the thermal insulation of the copper calorimeter is so good that the instrument loses heat at a rate of no more than 1.01% per hour at 20°C temperature above ambient. Since this cooling correction can be accurately measured, it introduces a relatively small error into everyday measurements. From Fig. 8 one can see it takes about 20 minutes for heat to diffuse throughout the body of

the copper cylinder and bring the temperature to within one part per thousand of its final value. This time only 100 sec for the silver block. The smaller time constant permits one to skimp on the thermal insulation requirement for this instrument since heating and stabilization generally occur in a few minutes. Experience obtained from operating the instruments over about two years shows that heater calibrations are reproducible to within  $\pm 0.25\%$  and  $\pm 0.5\%$  for the copper and silver calorimeters, respectively.

In March 1967 the copper calorimeter was checked against a 10.37-GeV electron beam whose integrated charge was measured directly by the Faraday cup. The intermediate transfer monitor was the precision beam current transformer.<sup>11</sup> From several measurements we conclude that the product of Beam Switchyard energy obtained from absolute magnetic measurements and a geometric survey (thought together to be accurate to 0.1%) and the charge integrated on a condenser calibrated against a standard traceable to NBS to 0.1%, is consistent with the electrical heater calibration (after photon and neutron energy loss corrections of 0.31% have been applied) to  $0.3 \pm 0.5\%$ . A major factor contributing to the then assigned  $\pm 0.5\%$  error is the fact that considerable care must be exercised with Faraday cup readings if even a small amount of material is in the beam path ahead of the cup. This material can give rise to photons that may subsequently remove electrons from the walls of the cup by Compton scattering and cause incorrect readings. One can estimate from later measurements on the thickness dependence of this effect that this error was about  $\pm 0.24\%$ . The silver calorimeter was also calibrated with 8 and 16 GeV electron beams. The results are shown in Fig. 10. Further, a direct comparison of the silver and copper calorimeters with each other using photon beams showed agreement to within 0.5%. However, the electrical heater calibrations of the silver calorimeter,

suitably corrected for photon and neutron losses, are consistently 2% too high. We believe that voids in the small silver block which result from the heater and thermometer wells, the cooling channels, and various casting holes may explain the discrepancy with the calculations. Calculation shows that it is not too important to strike the copper calorimeter dead center with the beam; the smaller silver instrument, however, must be more accurately located. The variation of silver calorimeter response with beam position is shown in Fig. 10. General properties of the instruments are summarized in Table 1.

### III. MINISEQ

#### A. Design

The MINISEQ is a secondary emission chamber with a front wall whose thickness is so chosen that the cascade shower induced by the incident beam develops nearly maximum multiplication over the range of beam energies under consideration.

Let us estimate the response of the MINISEQ when it is struck by a bremsstrahlung photon beam of an end point energy  $E_0$  with a total beam energy of  $U$ . If the MINISEQ contains  $m$  effective plates for secondary emission, the total amount of the electric charge  $q$ , collected by the foils of the MINISEQ, may be written

$$q = me N_0 \int \pi(E_0, E, t) \delta(E) dE \quad (\text{III.1})$$

where  $\delta(E)$  is the efficiency of secondary electron emission per plate when struck by an electron of energy  $E$ ,

$e$  is the charge of electron,

$N_0$  is the number of equivalent quanta =  $U/E_0$ ,

$\pi(E_0, E, t)$  : number of shower electrons of energy  $E$  at depth  $t$ .

## 1. Multiplication

For the total number of shower electrons of all energies  $\pi(E_0, t)$  per incident photon at depth  $t$  radiation lengths, shower theory under approximation B gives the following expression:<sup>17</sup>

$$\pi(E_0, t) = K(s, -s) \frac{H_\pi(s)}{\left\{ 2\pi \left[ \lambda_1''(s) t + ns^2 \right] \right\}^{1/2}} \frac{1}{s^n} \left( \frac{E_0}{\mathcal{E}_0} \right)^s e^{-\lambda_1(s)t} \quad (\text{III. 2})$$

where  $s$  the so-called "shower age" has been defined in the previous section, and  $K(s, -s)$ ,  $\lambda_1(s)$ ,  $\lambda_1''(s)$  and  $H_\pi(s)$  are functions of  $s$ , and their values are given by Rossi and Greisen.<sup>17</sup> As before  $n$  is a number which depends on the type of the incident particle and is equal to 1.5 for bremsstrahlung photons. Since shower maximum corresponds to  $s = 1$ , then  $\pi_{\max}(E_0)$ , the number of shower electrons at the maximum is given by the greatly simplified formula

$$\pi_{\max}(E_0) = \frac{0.31}{\left[ \ln \left( \frac{E_0}{\mathcal{E}_0} \right) - 0.37 n \right]^{1/2}} \left( \frac{E_0}{\mathcal{E}_0} \right) \quad (\text{III. 3})$$

a relation which implies that the multiplication  $\pi_{\max}$  is approximately proportional to the incident energy.

On the other hand, the absorber thickness  $T_{\max}$  where the shower curve maximum appears is given by the equation

$$T_{\max} = 1.01 \left[ \ln \left( \frac{E_0}{\mathcal{E}_0} \right) - n \right] \quad (\text{III. 4})$$

so that if  $E_0$  is sufficiently large compared to  $\mathcal{E}_0$ , the value of  $T_{\max}$  does not change very rapidly with incident energy. Furthermore, the shower curve has a very broad peak even for a given value of  $E_0$ .

We can expect, therefore, that the total number of shower electrons generated by the incident bremsstrahlung beam for constant depth of the absorber is very nearly a function of only the total beam energy  $U$  over some wide range of  $E_0$ . In fact  $\pi(E_0)/E_0$  from relation (III.2) is quite constant when plotted against  $E_0$  as shown in Fig. 11. The Monte Carlo calculation of this function at 6-GeV incident energy is lower by a factor of about 2. This calculation, however, has an electron cutoff energy of 1.5 MeV and we believe that shower electrons below this cutoff are also effective in contributing to the secondary emission process.

Because the secondary emission coefficient  $\delta$  is a function of incident electron energy we must know the spectrum of shower electrons as well. Fortunately, for a limited region of shower ages,  $\pi(E_0, E)$  can be written as a product of two functions

$$\pi(E_0) \cdot f(E)$$

where  $\pi(E_0)$  is the multiplication already discussed and  $f(E)$  is the spectral function.

At shower maximum  $f(E)$  has the following form:

$$f(E) = \frac{a}{(a + E)^2} \quad \text{(III.5)}$$

in which  $E$  is the energy of the electrons in MeV and  $a = 15.7$  MeV. This formula reproduces the energy spectrum obtained by Völkel's Monte Carlo calculations to within 20%.

## 2. Secondary Emission Coefficient

We use a curve presented by Ladage<sup>21</sup> for the energy dependence of the coefficient  $\delta(E)$ . The values for aluminum foil so obtained are multiplied by 1.14 which is the experimentally determined<sup>22</sup> emission ratio for gold-plated to pure aluminum surfaces. Since the spectral function  $f(E)$  is almost independent of  $E_0$

we can derive an average emission coefficient

$$\delta_{av} = \int \delta(E) f(E) dE \quad (\text{III. 6})$$

For a foil which can emit from its front and back surfaces, a numerical integration yields a value for  $\delta_{av}$  of 3.42% per foil.

### 3. Response of the MINISEQ

We are now in a position to insert values into Eq. (III. 1) to calculate the calibration constant of the instrument. If  $U$  the incident beam energy is expressed in joules, and  $q$  the total collected charge is in coulombs,

$$\frac{J}{q} = \frac{eU}{q} = \frac{eE_0(\text{GeV}) \times 10^9}{em \int \pi \delta} = \frac{eE_0(\text{GeV}) \times 10^9}{m\pi(E_0) \delta_{av}} \quad (\text{III. 7})$$

and following Ladage the effective number of emitters is 3, with 10 GeV incident photons we obtain approximately  $.8 \times 10^9$  joules per coulomb.

### B. Construction

The instrument is designed for up to 3 kW of beam power. A 3/4"-thick tungsten plate sandwiched between two water-cooled 1/4"-thick copper plates was chosen for the front wall of the MINISEQ. This corresponds to 5.63 radiation lengths and the effective value of  $\mathcal{E}_0$  (critical energy) for this composite material is estimated to be 9.8 MeV. Substituting this value of  $\mathcal{E}_0$  into Eq. (III.4), we find that the maximum multiplication for this front wall will occur for photons of 11.8 GeV end point energy.

The sensitive part of the detector consists of four high voltage electrodes and three collectors which are spaced alternately and separated by 1 mm. Gold-plated aluminum foils are used for each electrode in order to avoid changes in surface condition and to obtain higher sensitivity. The foils are 0.00017" thick

and are stretched on stainless steel frames. The frames are cooled by thermal conduction through alumina electrical insulators. The aperture is three inches. A 1/2"-thick tungsten plate sandwiched by two 1/4"-thick water-cooled copper plates is mounted as a backscatterer and absorber behind the secondary emission plates. The whole plate assembly is mounted in a stainless steel vacuum chamber which, by using ultrahigh vacuum techniques, is kept at around  $2 \times 10^{-9}$  torr by a 1 liter/sec ion pump. Minus 900 volts from a well-stabilized power supply is connected to the emitter plates. In order to derive a signal proportional to instantaneous beam intensity, as well as the normally integrated charge, in the latest type of MINISEQ, an additional collection chamber is mounted behind the other plates and its collector is brought out via a separate terminal.

### C. Operation

The radial distribution of the sensitivity of the MINISEQ was measured by comparing its response as a function of position with that of a fixed SEM. A 16-GeV incident electron beam was used whose size was less than 1 cm in diameter at the position of the MINISEQ. The device was shifted laterally with respect to the beam by means of its trolley. The results are shown in Fig. 12. Although a flat distribution cannot be expected from such a small chamber because of the lateral spread of the shower, 1 cm displacements of the center of gravity of the beam within the usually employed 1 cm high by 2 cm wide collimator hole cannot cause errors greater than 1%.

During photoproduction experiments absolute calibrations of the MINISEQ were frequently made at various energies against the silver calorimeter and checked occasionally against the copper calorimeter, using the Cerenkov monitor as an intermediate standard. Figure 13 shows the long term stability of the

calibration constant of the MINISEQ,  $J/q$ . The reader may note that we have defined this constant to be inversely proportional to the instrument's sensitivity. As seen from the figure, there seems to be a gradual increase (about 2%) in the sensitivity over one month. One may attribute this variation to the changes of the surface condition of the foils. For short time stability, however, at each energy reproducibility of the calibration constant was generally found to be within  $\pm 0.6\%$ .

In Fig. 14, the calibration constants of the MINISEQ are plotted as a function of end point energy  $E_0$  of the incident bremsstrahlung beam. Data are divided into three groups according to the time period during which data were taken. The solid curve in this figure shows the average measured energy dependence of the calibration constant. The sensitivity of the MINISEQ varies only by 2.0% over the range of  $E_0$  from 8 GeV to 18 GeV. A rapid rise of the calibration constant below 8 GeV may be the result of the fact that showers induced by such low energy beams are behind the shower-curve maximum at the position of the secondary emission plates. For comparison, the calculated energy variation of the MINISEQ is shown in Fig. 14 by a dashed curve. It has been normalized to the experimental points at 10 GeV. This curve, of course, reflects only the variation of  $\pi(E_0)$  with  $E_0$ . Also shown is an electron beam calibration performed five months later.

Three comments may be made regarding normalization:

1. As pointed out by Yuda et al.,<sup>23</sup> the total number of shower electrons expected from Eq. (III.2) is rather higher than the observed values because complete screening cross sections were used for pair production and bremsstrahlung processes over the whole range of shower particles.

2. Due to the small lateral dimensions of the MINISEQ, some number of shower electrons likely flow out the side wall without striking all of the secondary

emission foils. This is particularly true of the very low energy electron component which is nearly isotropic and which we have included in our calculation but which are omitted in the previously mentioned Monte Carlo calculations.

3. Secondary emission coefficients are notoriously sensitive to the conditions under which the gold is evaporated on the foils. Variations of 20% are observed by Dell and Fotino<sup>24</sup> for example.

Considering the above and other approximations inherent in shower theory, we feel that the measured absolute response of the instrument,  $1.3 \times 10^9$  joules per coulomb, agrees as well as can be expected with that calculated in Section III.A, namely  $0.8 \times 10^9$ .

#### IV. CERENKOV PHOTON BEAM MONITOR

##### A. Design

A Cerenkov-light photon beam monitor, consisting of a gas cell preceded by a thin radiator and containing an optical system for collecting and measuring the light flux, can be made insensitive to low energy particle spray accompanying the beam, if the index of refraction of the gas can be made sufficiently small so that these low energy particles are below Cerenkov threshold in the medium. Let us estimate the response of such a monitor.

For small angles  $\theta$  and values of  $n$ , the index of refraction, close to one, the Cerenkov relation  $\cos \theta = 1/\beta n$  may be approximated by

$$\theta^2 \approx 2\eta - \frac{1}{\gamma^2} \quad (\text{IV. 1})$$

where  $\eta = n-1$  and  $\gamma^2 = 1/1-\beta^2$ , from which one can see that the critical energy below which no light is emitted is

$$\gamma_c = \frac{1}{\sqrt{2\eta}} \quad (\text{IV. 2})$$

and the maximum angle in the cell, due to the highest energy electron from the radiator is

$$\theta_n = \sqrt{2\eta} \quad (\text{IV.3})$$

The number of photons produced by a single particle per cm of path in the spectral range 3500 Å to 5000 Å is<sup>25</sup>

$$N_\phi = 390 \theta^2 \quad (\text{IV.4})$$

so that we can write by combining 1, 2 and 4

$$N_\phi = 390 \ell \left( 2\eta - \frac{1}{\gamma} \right) = 390 \ell \left( \frac{1}{\gamma_c} - \frac{1}{\gamma} \right)$$

To calculate the number of electrons of energy  $\gamma$  we must fold together the number of photons in the bremsstrahlung spectrum with their probability of making pairs in the thin radiator. Assume that the energy spectrum of the gamma-ray flux is of the form

$$dN(k) = N_0 \frac{dk}{k} \quad (\text{IV.5})$$

in which  $N_0$ , the number of "equivalent quanta" per second may be replaced by

$$N_0 = 6.25 \times 10^{12} \frac{P}{K_m} \quad (\text{IV.6})$$

where  $P$  is the power of the beam in kilowatts and  $K_m$  is the "end point" energy in GeV.

Assume further that the electron energy spectrum resulting from the conversion of a photon of energy  $k$  in the radiator is equally populated from 0 to  $k$ . This means that the probability of finding an electron in the energy range  $d\gamma$  will vary as  $T/k$ , where  $T$  is the thickness of the radiator in radiation lengths.

Assuming further that the pair production cross section is constant over the range of energies of interest, we can calculate the number of electrons per second of energy  $\gamma$  in the range  $d\gamma$

$$dN_e(\gamma) = 2 \times \frac{7}{9} T \int \frac{dN(k)}{k} d\gamma = 10^{13} \frac{PT}{K_m} d\gamma \int_{k=\gamma}^{k=\gamma_{\max}} \frac{dk}{k^2} = 10^{13} \frac{PT}{K_m} \left[ \frac{1}{\gamma} - \frac{1}{\gamma_{\max}} \right] d\gamma \quad (\text{IV.7})$$

The lower limit obtains from the photons' necessity of having at least energy  $\gamma$  to produce a charged particle of such energy. The total number of Cerenkov photons per second is

$$N_\phi = 390 \times 10^{13} \frac{PT\ell}{K_m} \int_{\gamma_c}^{\gamma_{\max}} \left( \frac{1}{\gamma_c} - \frac{1}{\gamma} \right) \left( \frac{1}{\gamma} - \frac{1}{\gamma_{\max}} \right) d\gamma \quad (\text{IV.8})$$

The resulting integration may be simplified to

$$\frac{1}{\gamma_c} \left[ \ln \left( \frac{\gamma_m}{\gamma_c} \right) - \frac{3}{2} + 2 \frac{\gamma_c}{\gamma_m} - \frac{1}{2} \frac{\gamma_c^2}{\gamma_m^2} \right]$$

and in our design in which  $\gamma_c/\gamma_m \ll 1$  we neglect the last two terms. Replacing  $\gamma_c^2$  by  $2\eta$  the Cerenkov photon flux is

$$N_\phi = 7.8 \times 10^{15} \frac{PT\ell\eta}{K_m} \left[ \ln \left( \frac{\gamma_m}{\gamma_c} \right) - \frac{3}{2} \right] \text{sec}^{-1} \quad (\text{IV.9})$$

which when multiplied by the average photon energy of  $2.9 \text{ eV} = 4.6 \times 10^{-19}$  joules yields a light power

$$P_\phi = 3.6 \times 10^{-3} \frac{PT\ell\eta}{K_m} \left[ \ln \frac{\gamma_m}{\gamma_c} - \frac{3}{2} \right] \text{watts} \quad (\text{IV.10})$$

Inserting values for a 1 m long helium-filled cell  $l = 100$  cm,  $T = 10^{-3}$  radiation lengths and  $\eta = 3.5 \times 10^{-5}$  (at 1 atmosphere), we find that the critical energy for an electron in the counter is 60 MeV and

$$P_{\phi} = 1.25 \times 10^{-8} \frac{P}{K_m} \left[ \ln K_m + 1.32 \right] \text{ watts} \quad (\text{IV.11})$$

For  $K_m = 10$  GeV this relation yields Cerenkov light power of  $4.6 \times 10^{-9}$  watts per incident kilowatt of gamma rays.

If we wish to monitor a gamma-ray beam of say 30 watts with a signal-to-noise ratio of 1000:1 this means the photomultiplier must have an equivalent anode dark current input of no more than

$$0.03 \times 4.6 \times 10^{-9} \times 10^{-3} = 1.4 \times 10^{-13} \text{ watts} .$$

## B. Construction

From Fig. 4 we see that the monitor is simply a flanged aluminum tube with very uniform 0.005" aluminum windows at each end which may be remotely evacuated and filled with about 1 atmosphere of helium. The pressure is monitored by a gauge<sup>26</sup> to 1 mm Hg. The opaque baffle is parallel to the plane of the mirror so that the active length  $l$  is insensitive to the position of the beam. The baffle and mirror which are normally at  $45^\circ$  to the beam may be remotely flipped out by means of an air driven actuator. They are made by stretching 0.001" thick aluminum-coated mylar onto circular frames. The baffle is then carefully sprayed with flat black paint. Cerenkov light, reflected downward by the mirror, is focused by a quartz lens onto the face of an integrating photomultiplier tube. The lens itself provides the vacuum seal. Located between the lens and the tube is a diffuser insuring more uniform illumination and hence, one hopes, less sensitivity to variations in beam position. The diffuser introduces a light loss of a factor of 2.

The anode output from the photomultiplier is connected directly to an integrator via 300' of cable whose capacitance acts as a high frequency filter. Care has been taken to keep the tube base current sufficiently high, about 3.5 mA, so that peak currents, which stem from the low duty cycle of the beam, do not introduce nonlinearities. The tube's high voltage is monitored continuously.

It was found very convenient during an experiment to have knowledge of the time distribution of the photon beam pulse. Rather than divide the signal from the integrating phototube, another photomultiplier tube was added which samples Cerenkov light scattered from the diffuser.

In addition to the dark current inherent in the tube due to thermal noise, stray radiation from room background will lower the signal-to-noise ratio. This background comes primarily from the fact that the main beam is absorbed in the MINISEQ located only 7 meters downstream, but it can be reduced to tolerable levels by surrounding the tubes with a lead shield about 8" thick.

The total thickness this monitor introduces into the beam is 0.00314 radiation lengths. Since photons converted to electrons in any radiator upstream of the target are not effective in producing pions in the target but will contribute to total energy as measured by the calorimeter, a correction for this effect must be applied. In fact the major contribution to this correction comes from the thickness of the hydrogen target itself.

### C. Operation

Figure 15 shows the inverse response of the monitor in joules (transmitted) per coulomb (collected). The dotted curve is that expected from the relation (IV.11) of the previous section normalized to the experimental points at 10 GeV.

As mentioned in the above sections, the signal-to-noise ratio is determined by two factors, thermal noise in the tube and beam-induced room background. The former sets a lower limit on the photon flux that can be measured but can in principle be removed by either cooling the tube or performing a subtraction proportional to the elapsed time of a run. This contribution is measured with the beam off and was not found to limit the instruments' performance at the power levels of interest in our experiments. Beam-induced room background is measured either by pumping out the gas or flipping the mirror out of the beam. Either method yielded the same result indicating that this background is not sensitive to the gas. Signal-to-noise ratios under normal running conditions were generally (600 to 1000)/1.

During early operation of this instrument several interesting problems came to light. First, it was noticed that the spread in calibration values obtained during operation of an experiment was greater at higher photon beam energies. This effect was traced to the fact that both primary and secondary collimators were too thin. They were 30 radiation lengths thick. When tungsten edges were added to the downstream ends of the high power slits which had originally been designed on the basis of thermal protection of downstream components and the anti-halo scraper was thickened to 80 radiation lengths of tungsten, it was possible to missteer the beam to the extent that one half its power was lost on the collimators without affecting the calorimetrically determined calibration of the Cerenkov monitor by more than about 2% at all incident energies. For steering changes of this order, the ion chamber and SEM monitors, which are sensitive to collimator spray would show up to 25% variations. It was also noticed that the calibration constant appeared to change by 7% with a time constant of about 15 minutes after the beam was turned on after having been off for periods greater than one hour.

This effect was traced to a fatigue effect in the integrating phototube and could be reproduced in the laboratory with a calibrating lamp.

Following the discussion in Section IV.A on dark current requirements, a 14-stage 8575 bi-alkali cathode tube with a noise figure of  $4 \times 10^{-15}$  watts had been originally selected. Several tubes of this type showed the same fatigue effects. It was not possible, however, to find the effect with 10-stage type 6342 tubes and one of these, specially selected for low noise, was installed and operated successfully for a year. Under steady running conditions, reproducibility of calibrations was generally within  $\pm 1\%$  over periods of many hours. Recently, following an accident, this tube was replaced and the monitor now appears to behave nonlinearly at high photon beam intensities, reproducibility displaying an increase in gain of 1.8% when the beam intensity is increased from 1 to  $2 \times 10^9$  equivalent quanta per pulse. The effect appears to be related to the magnitude of the tubes' output current, but is not understood at this time. Clearly a monitor that rests on the gain stability of a photomultiplier tube will not have as good long term reproducibility as the other instruments of this system. For instance, a 1.8% variation will result from a high voltage power supply drift of one volt in a thousand. Fortunately, there are so many on-line checks during the running of an experiment, that whenever a suspect monitor ratio appeared, it was possible to insert either the MINISEQ or the calorimeter to check performance. The trolley cars on which the instruments are mounted can be moved into place in fractions of a minute and easily placed with an accuracy of  $\pm 1/16''$ . Zinc sulphide screens on the instruments' center line provide additional checks on beam position.

## V. SUMMARY

We have described in the foregoing the design, construction and operational experience of a system of three types of instruments — calorimeters, small secondary emission quantimeters and a Cerenkov light monitor that were used to measure the intensity of a high power photon beam in connection with a series of photoproduction experiments at SLAC. In general the instruments behave in a manner predicted by design. The copper calorimeter laboratory standard we believe, with careful use, should permit absolute total energy measurements to be made to an accuracy of better than  $\pm 0.5\%$  over a period of several years. The more convenient silver calorimeter has a greater energy dependence and because of its smaller thermal capacity is better used at photon fluxes corresponding to a few hundred watts. Our every day monitor, the MINISEQ, is found, when measured against the calorimeters to have a calibration constant reproducible to within  $\pm 1\%$  over a period of weeks. As a thin nondestructive instrument the Cerenkov monitor fulfills our hope of not being overly sensitive to low energy spray from the collimators. This monitor, depending as it does on the stability of a phototube needs to be checked every few hours or in the event of radically altered beam conditions, if it is to be trusted at the one percent level.

It is a pleasure to be able to acknowledge the help given us by other members of SLAC Experimental Group C under the direction of Dr. B. Richter, the operating staff of the accelerator and particularly the engineering talents and dedicated efforts of E. Roskowski, L. Karvonen, M. Lateur and R. Culver. Dr. J. R. Rees performed the basic design calculation for the Cerenkov monitor.

## REFERENCES

1. A. M. Boyarski *et al.*, Phys. Rev. Letters 20, 300 (1968) and 22, 148 (1969).
2. R. A. Early, "A thick target bremsstrahlung program," Report No. SLAC-TN-66-15, Stanford Linear Accelerator Center, Stanford University, Stanford, California (1966); unpublished.
3. E.g., see N.R.S. Tait, Nucl. Instr. and Methods 67, 56 (1969); and G. Lutz and H. D. Schulz, DESY Report No. 67/29 (1967).
4. R. R. Wilson, Nucl. Instr. and Methods 1, 101 (1957).
5. H. Fischer and C. Schaerf, Rev. Sci. Instr. 35, 615 (1964); and R. Anderson, "SLAC high power quantameter," Report No. SLAC-PUB-413, Stanford Linear Accelerator Center, Stanford University, Stanford, California (1968).
6. Y. Murata and S. Watanabe, Report No. INS-TH-53, Institute for Nuclear Study, University of Tokyo, Tokyo, Japan (1966).
7. P. D. Edwards and D. W. Kerst, Rev. Sci. Instr. 24, 490 (1952); and R. Anderson and B. Richter, "Calorimeter for absolute photon and electron beam energy determination," Report No. SLAC-TN-66-21, Stanford Linear Accelerator Center, Stanford University, Stanford, California (1966).
8. F. W. Martin, Thesis, Gutenberg University, Mainz, Germany (1966); and A. Ladage and P. Pingel, DESY Report No. 65/12 (1965).
9. H. H. Nagel, Z. Physik 186, 319 (1965); U. Völkel, DESY Report No. 65/6 (1965) and DESY Report No. 67/16 (1967); and H. Burfeindt, DESY Report No. 67/24 (1967).
10. E. J. Seppi, J. K. Cobb and D. R. Jensen, IEEE Transactions on Nuclear Science NS-14, 473 (1967); and H. Weidner, E. J. Seppi and J. Harris, IEEE Transactions on Nuclear Science NS-14, 918 (1967).

11. R. S. Larsen and D. Horelick, Proceedings of the Symposium on Beam Intensity Measurement, Daresbury Nuclear Physics Laboratory, Warrington, Lancs., England (April 1968); p. 260.
12. D. Yount, Nucl. Instr. and Methods 52, 1 (1967).
13. C. J. Crannell, H. Crannell and H. D. Zeman, Report No. HEPL-530, High Energy Physics Laboratory, Stanford University, Stanford, California (September 1967).
14. Cary Type 31, Cary Instrument Company.
15. H. DeStaebler et al., "Reduction of the thermal neutron flux in concrete using paraffin moderators," Report No. SLAC-TN-65-11, Stanford Linear Accelerator Center, Stanford University, Stanford, California (1965).
16. W. R. Nelson, T. M. Jenkins, R. C. McCall and J. Cobb, Phys. Rev. 149, 201 (1966).
17. B. Rossi and K. Greisen, Rev. Mod. Phys. 13, 240 (1941).
18. Firerod-Model G5A8, Watlow Electric Company.
19. Model 104P, Rosemount Engineering Company.
20. C. W. Ross, AIEE Joint Nuclear Instrumentation Symposium, Raleigh, N.C., (September 1961); paper 5-4.
21. A. Ladage, DESY Report No. 65/16 (1965).
22. S. A. Blankenburg, J. K. Cobb and J. J. Murray, IEEE Particle Accelerator Conference, Washington, D.C. (March 1965).
23. T. Yuda, A. Masaike, A. Kusumegi, Y. Murata, I. Ohta and J. Nishimura, to be published.
24. T. F. Dell and M. Fotino, Report No. CEAL 1045, Cambridge Electron Accelerator (November 1968).
25. J. V. Jelly, Cerenkov Radiation (Pergamon Press, Long Island City, N.Y., 1958); p. 230.
26. Model FA 129160, Wallace and Tiernan, Inc., Belleville, New Jersey.

TABLE 1

Properties of calorimeters	Unit	Copper	Silver
Diameter	cm	25.4	12.5
Length	cm	50.8	21.0
Diameter Molière units	--	8.54	4.1
Length in radiation lengths	$X_0$	38.0	24.5
Time to settle after heating	seconds	1300	100
Heater power (max)	kW	2.0	.5
Time to cool with water flowing	minutes	12	2
Tolerance of beam position	inches	$\pm 1.0$	$\pm 0.25$
Electrical calibration constant	$^{\circ}\text{C}/\text{MJ}$	$11.58 \pm 0.05$	$195.6 \pm 0.5$
10.3 GeV electron calibration constant	$^{\circ}\text{C}/\text{MJ}$	$11.51 \pm 0.5$	--
8 GeV electron calibration constant	$^{\circ}\text{C}/\text{MJ}$	--	$189.4 \pm 1$
16 GeV electron calibration constant	$^{\circ}\text{C}/\text{MJ}$	--	$188.7 \pm 1$

## LIST OF FIGURES

1. Layout of photon beam components in the SLAC beam switchyard and End Station A.
2. Cutaway drawing of MINISEQ showing mounting and shielding arrangement.
3. Cutaway drawing of the silver and copper calorimeters.
4. Schematic drawing of the Cerenkov light photon beam monitor.
5. % energy loss  $F(s)$  as a function of depth, in units of "shower age"  $s$ , for radii corresponding to the silver and copper calorimeters. The operating points of the two devices are shown for bremsstrahlung photons by arrows.
6. % energy loss  $F(s)$  for the silver calorimeter as a function of incident energy  $E$  of either bremsstrahlung or electron incident beam.
7. Diagram of electrical instrumentation for either calorimeter.
8. Typical response of the copper calorimeter to heat inputs during calibration runs. The insert table lists values of parameters used. The calibration constant  $\Delta T/MJ$  has units of degrees centigrade temperature rise per megajoule.
9. The variation of the "constant"  $\alpha$ , (used in reducing temperature readings) as a function of the average temperature of a calorimeter.
10. The silver calorimeter calibration constant as a function of incident beam position. The electron beam was about 1 cm in diameter for this measurement.
11. Plot of the normalized shower multiplication  $\pi(E_0)/E_0$  for a constant depth  $t = 5.63$  radiation lengths, the effective  $\mathcal{E}_0$  for the sandwich is 9.8 MeV (see text).
12. Response of the MINISEQ as a function of beam position. Normalized with respect to a 6" oscillating secondary emission monitor.

13. Variation of the MINISEQ calibration constant as a function of time at various bremsstrahlung end point energies. Pressure inside the vessel was always less than  $2 \times 10^{-9}$  torr.
14. Response of the MINISEQ as a function of energy — data taken at various times. The solid curve is drawn only as a guide to the eye. The dotted line is the energy dependence expected from the calculation outlined in the text and normalized at 10 GeV.
15. Response of the Cerenkov monitor vs end point energy of the photon beam. The dotted curve is calculated from relation (IV.11) in the text, normalized at 10 GeV for arbitrary gain of the phototube.

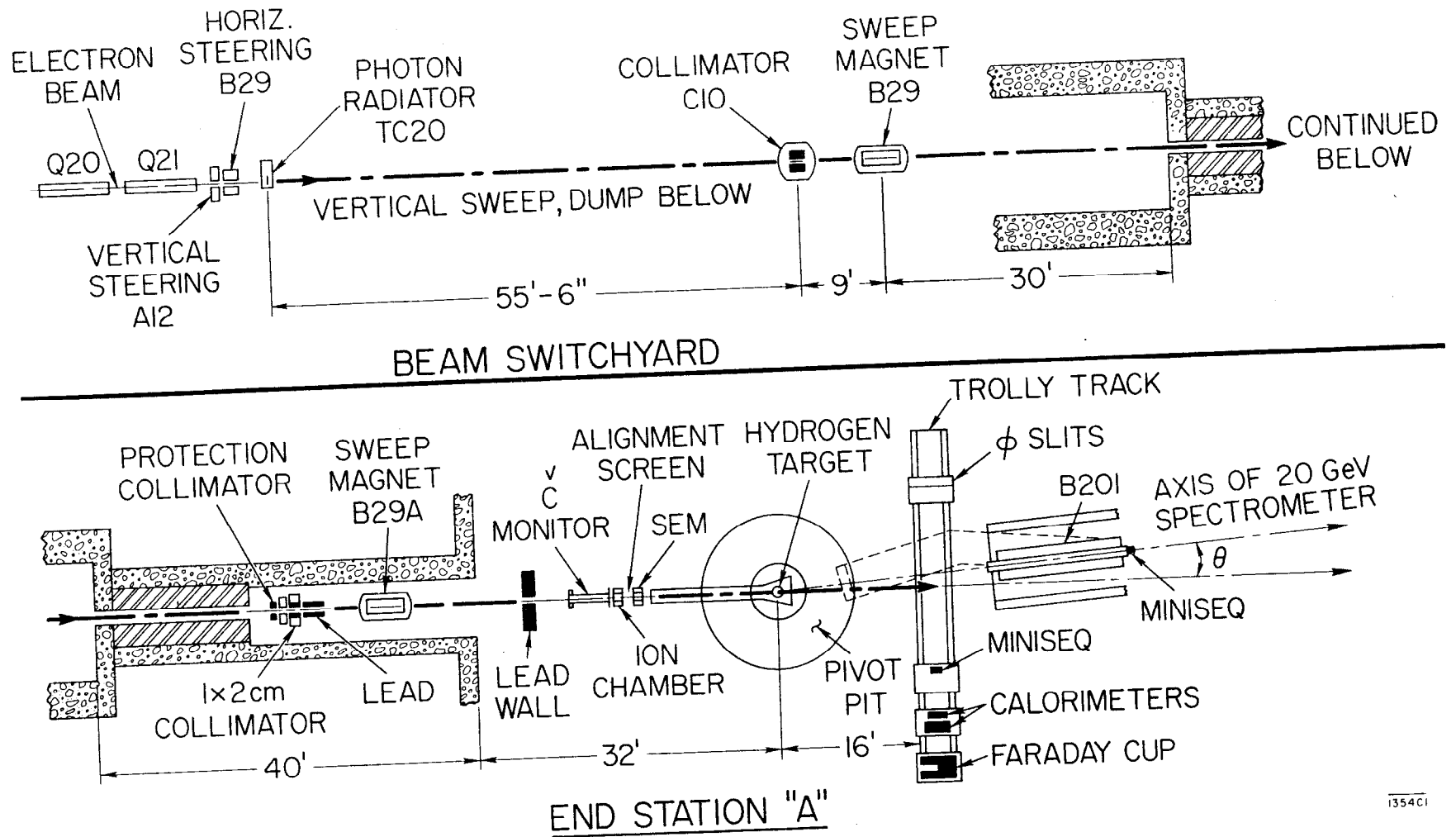


Fig. 1

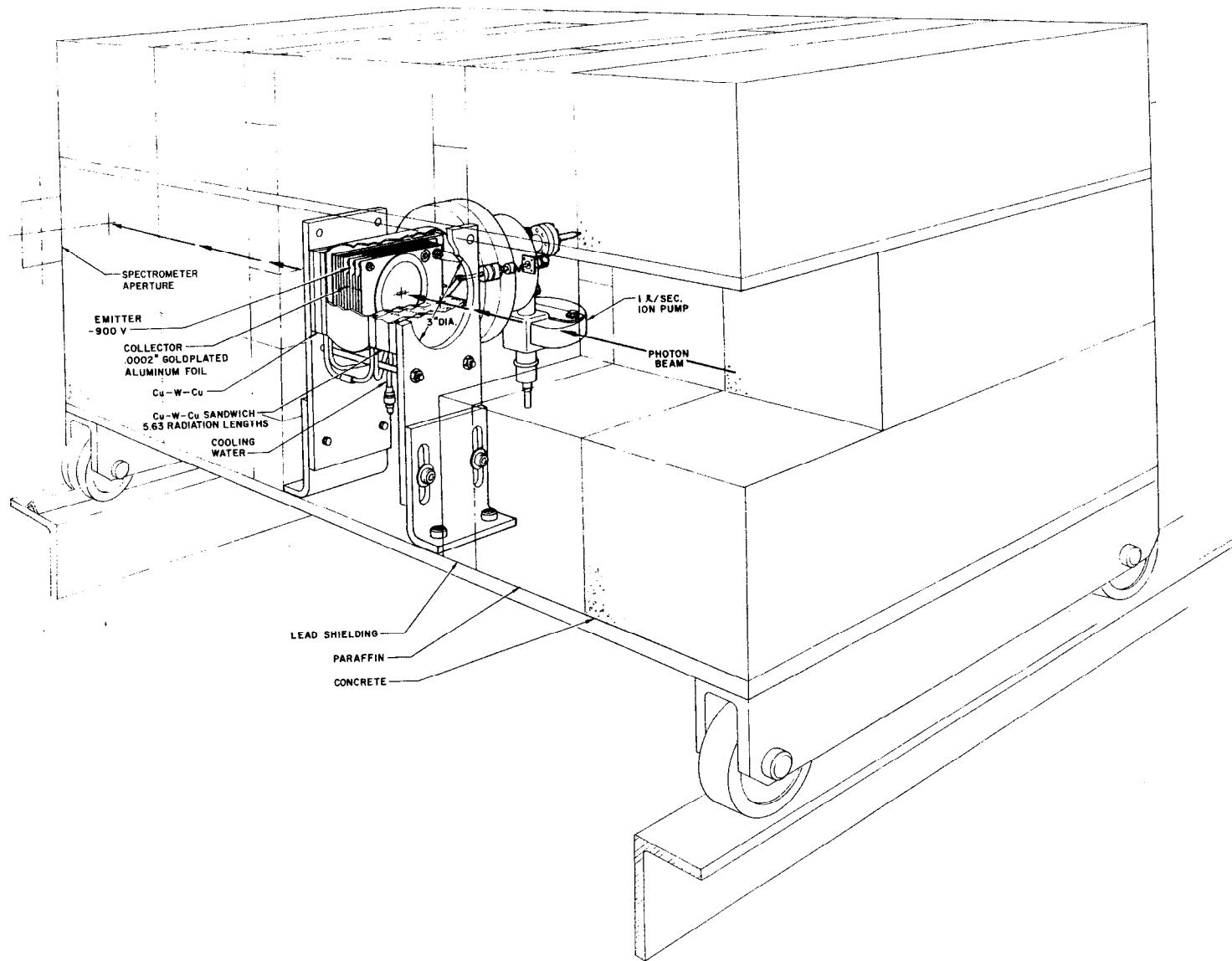


Fig. 2

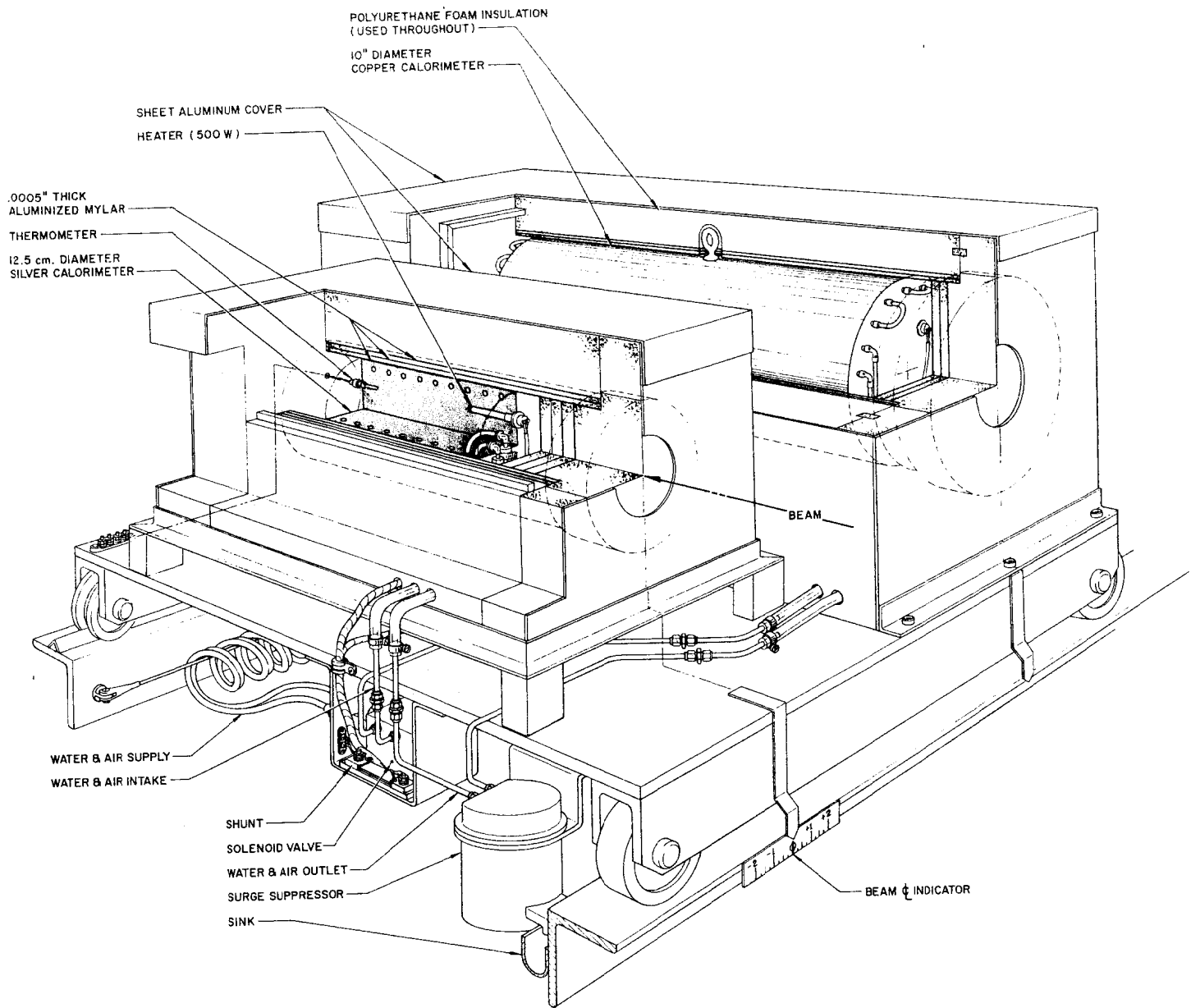
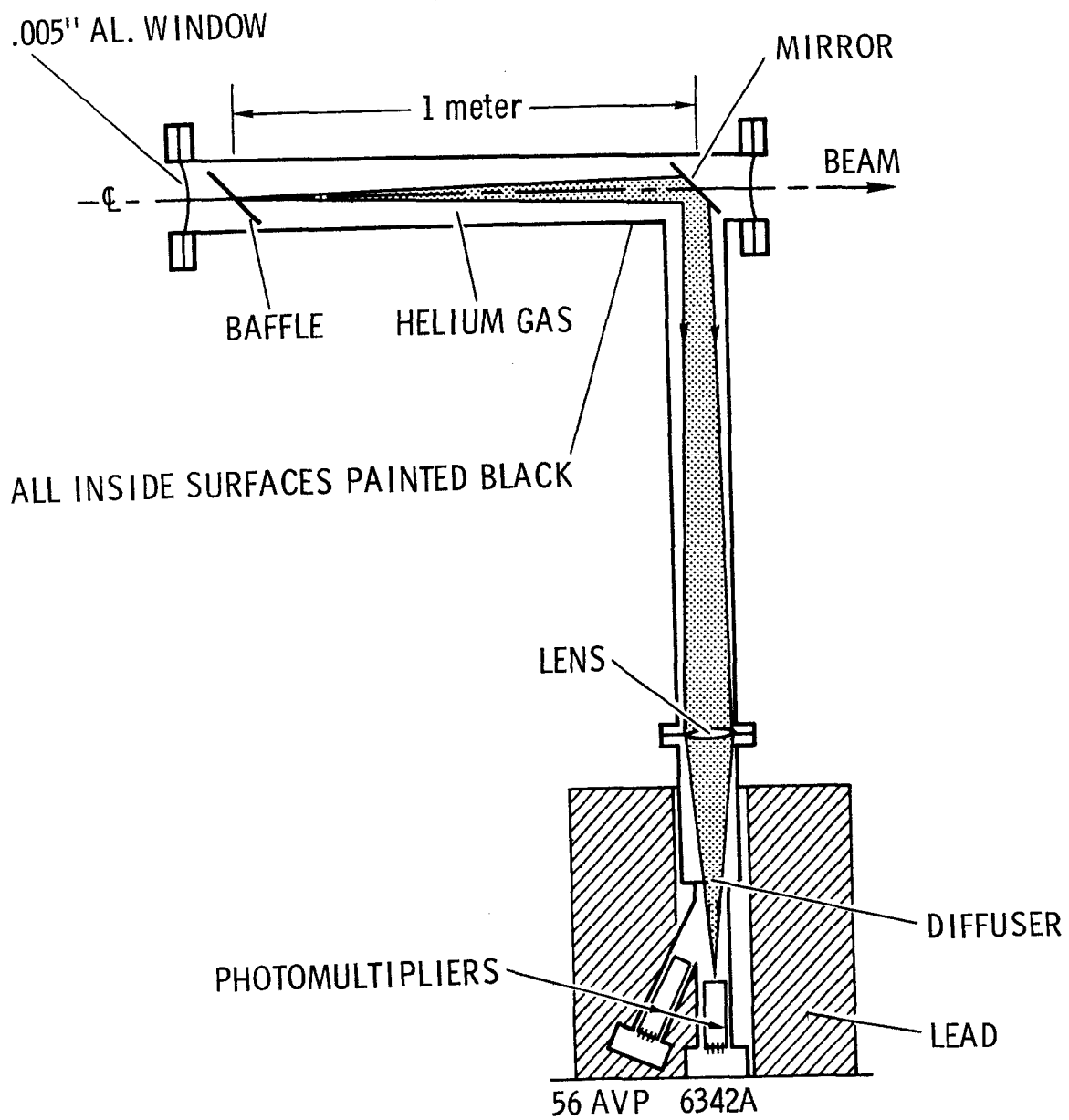


Fig. 3



1354A4

Fig. 4

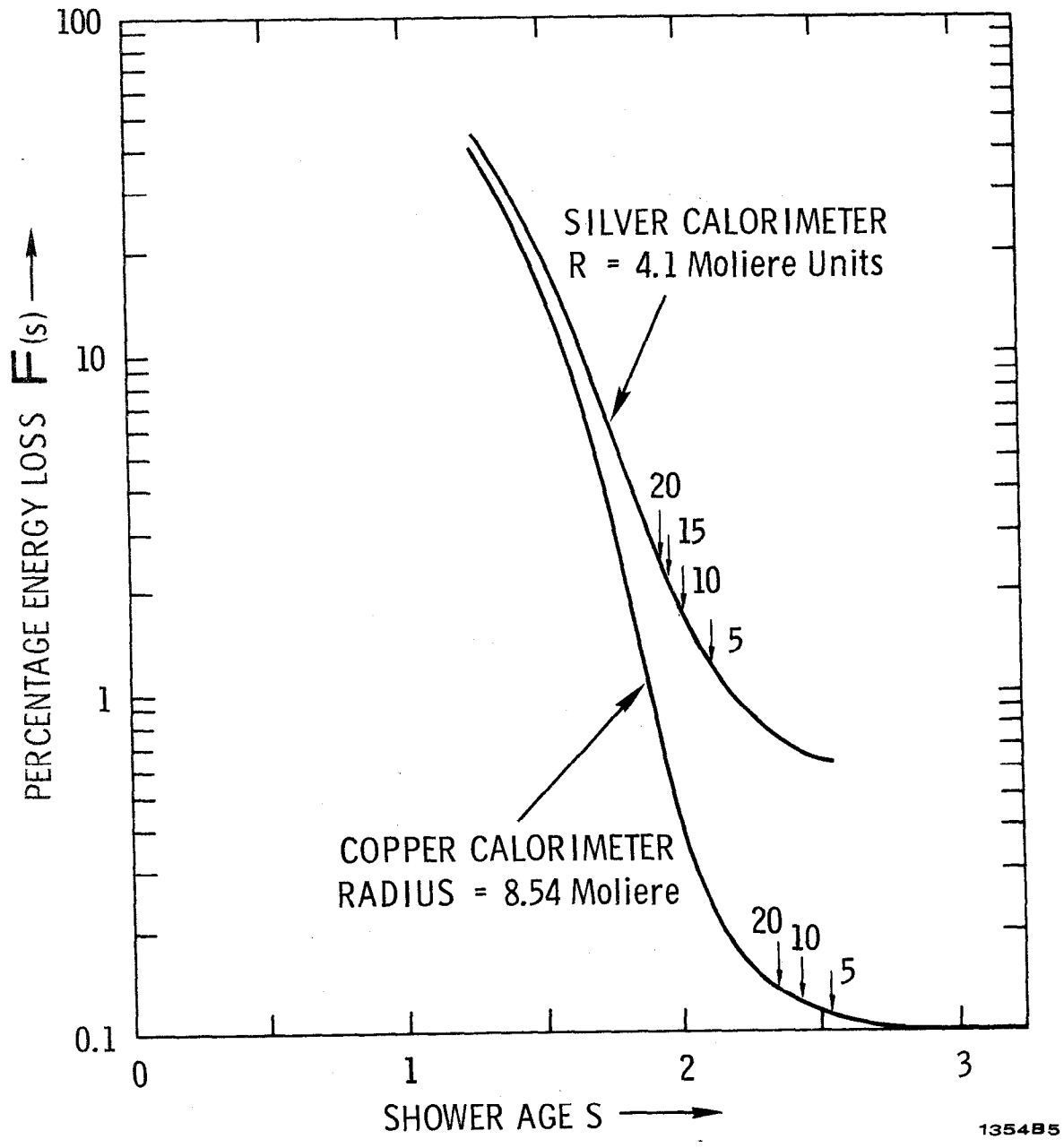


Fig. 5

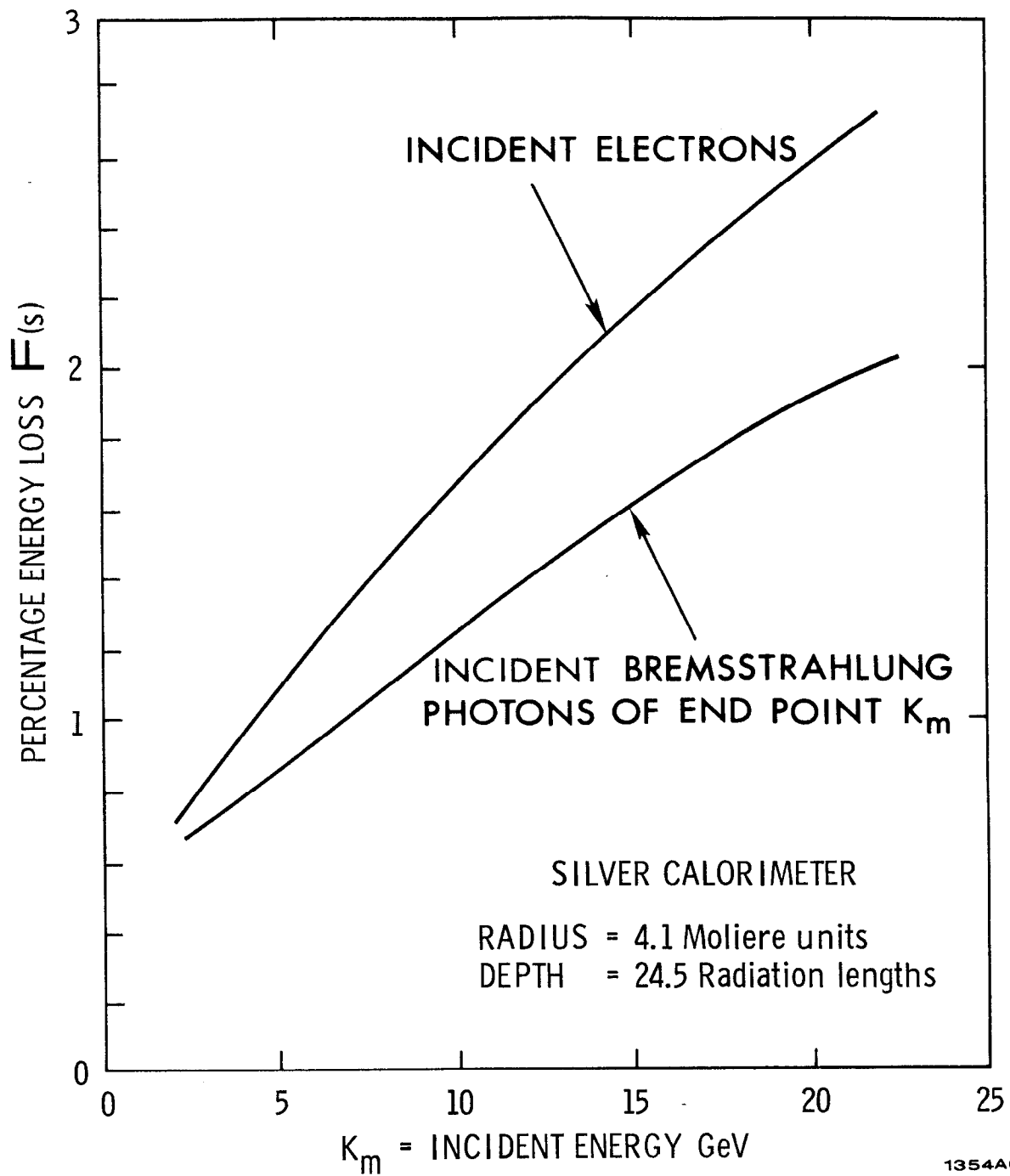
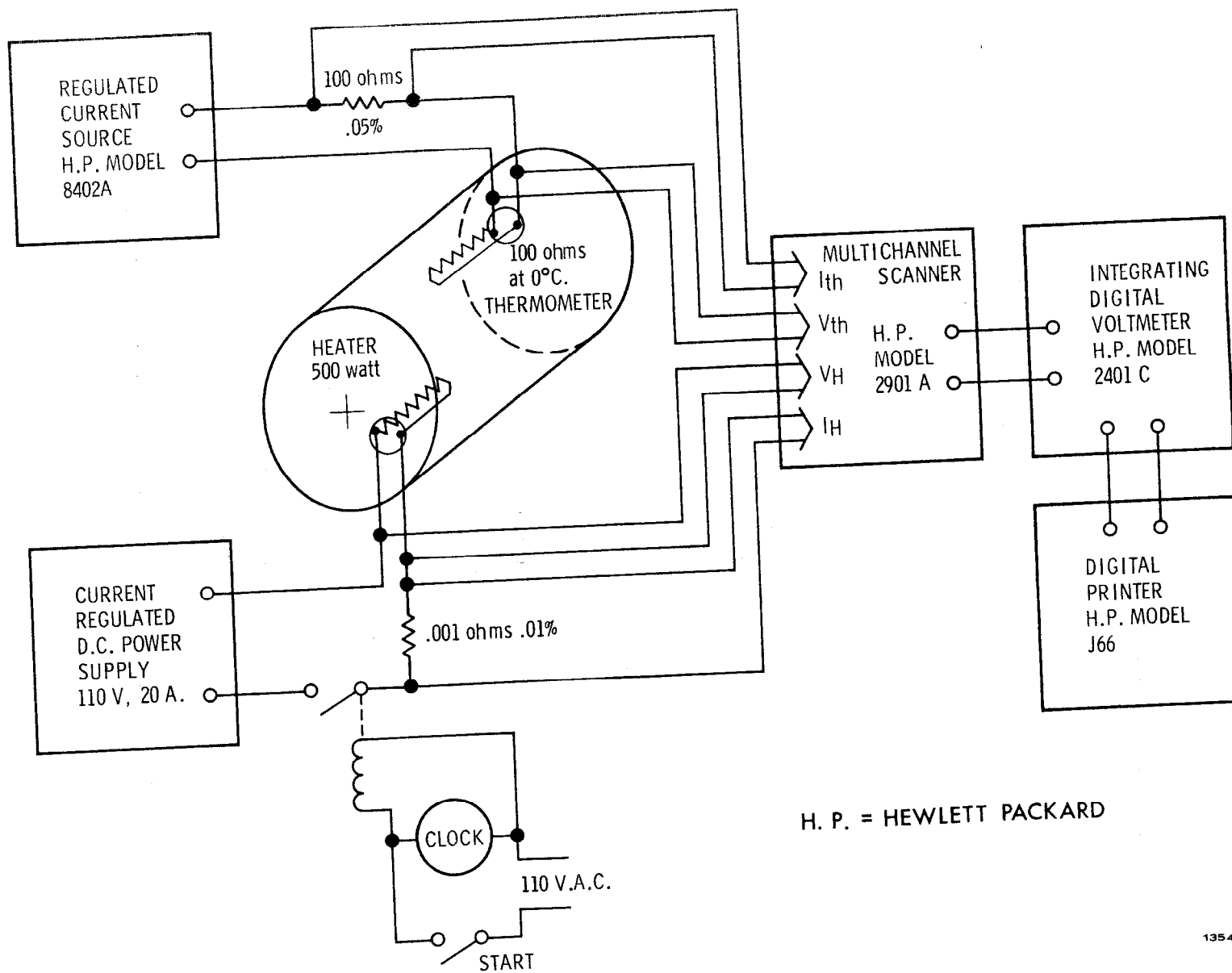


Fig. 6



135487

Fig. 7

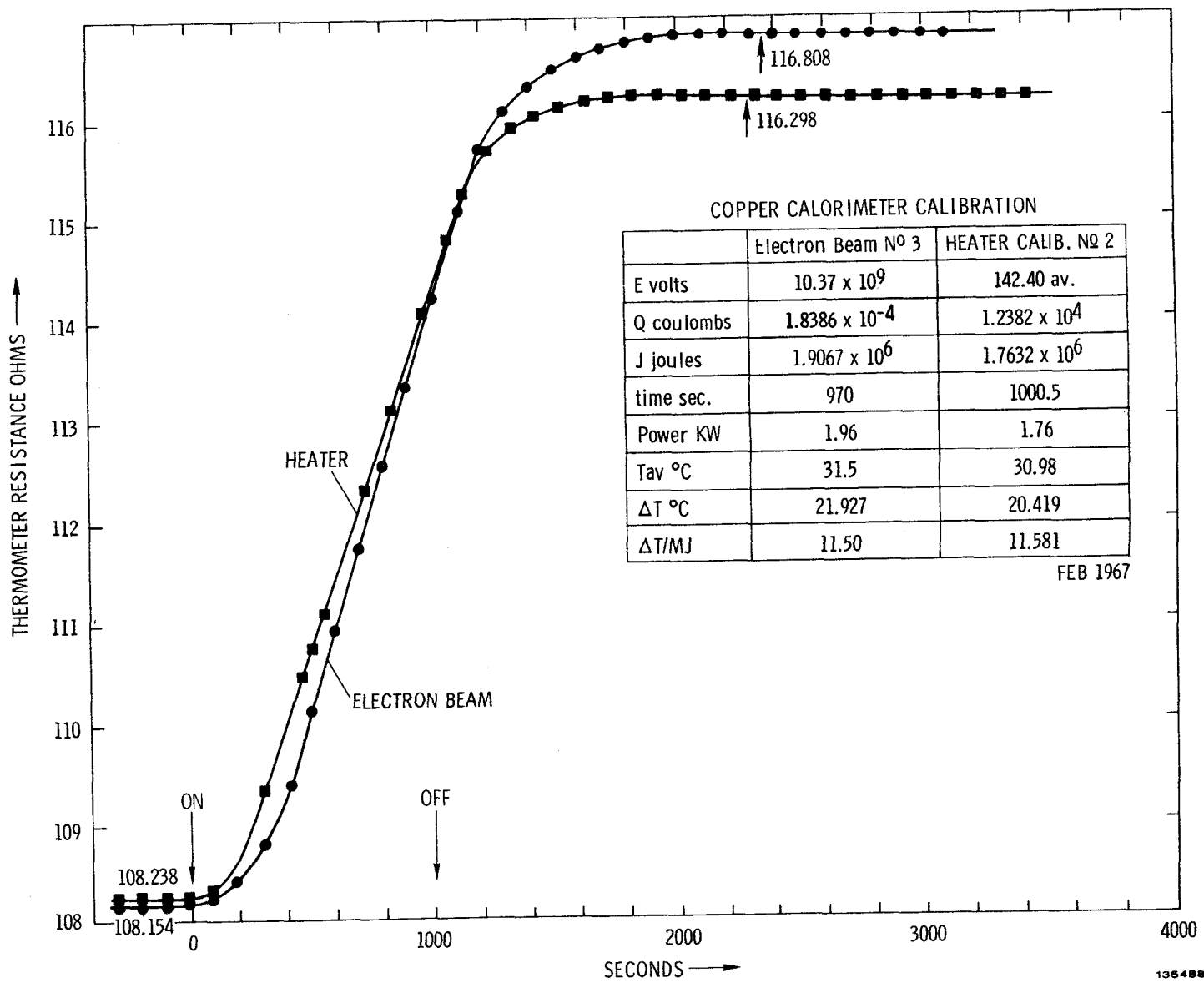


Fig. 8

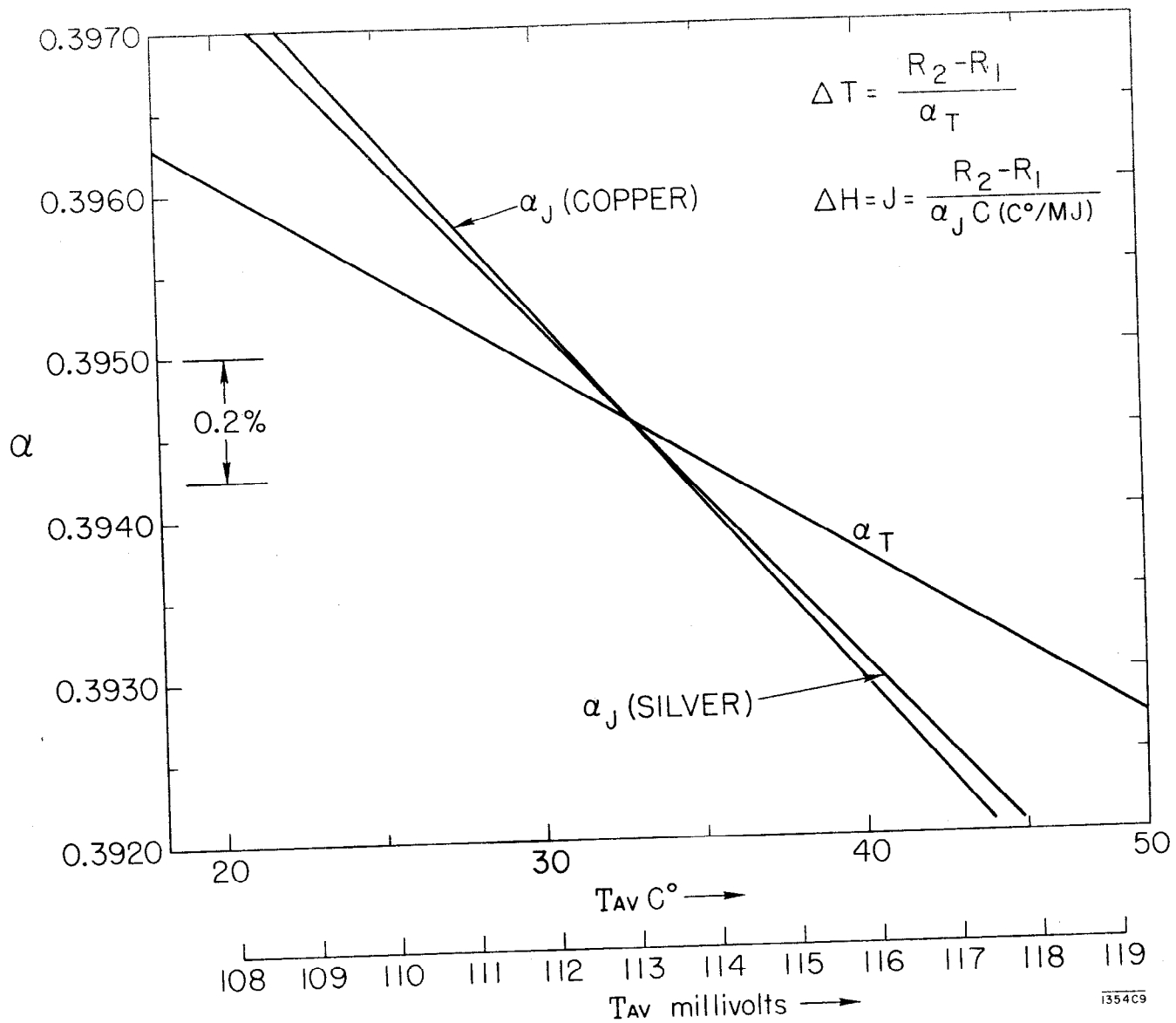
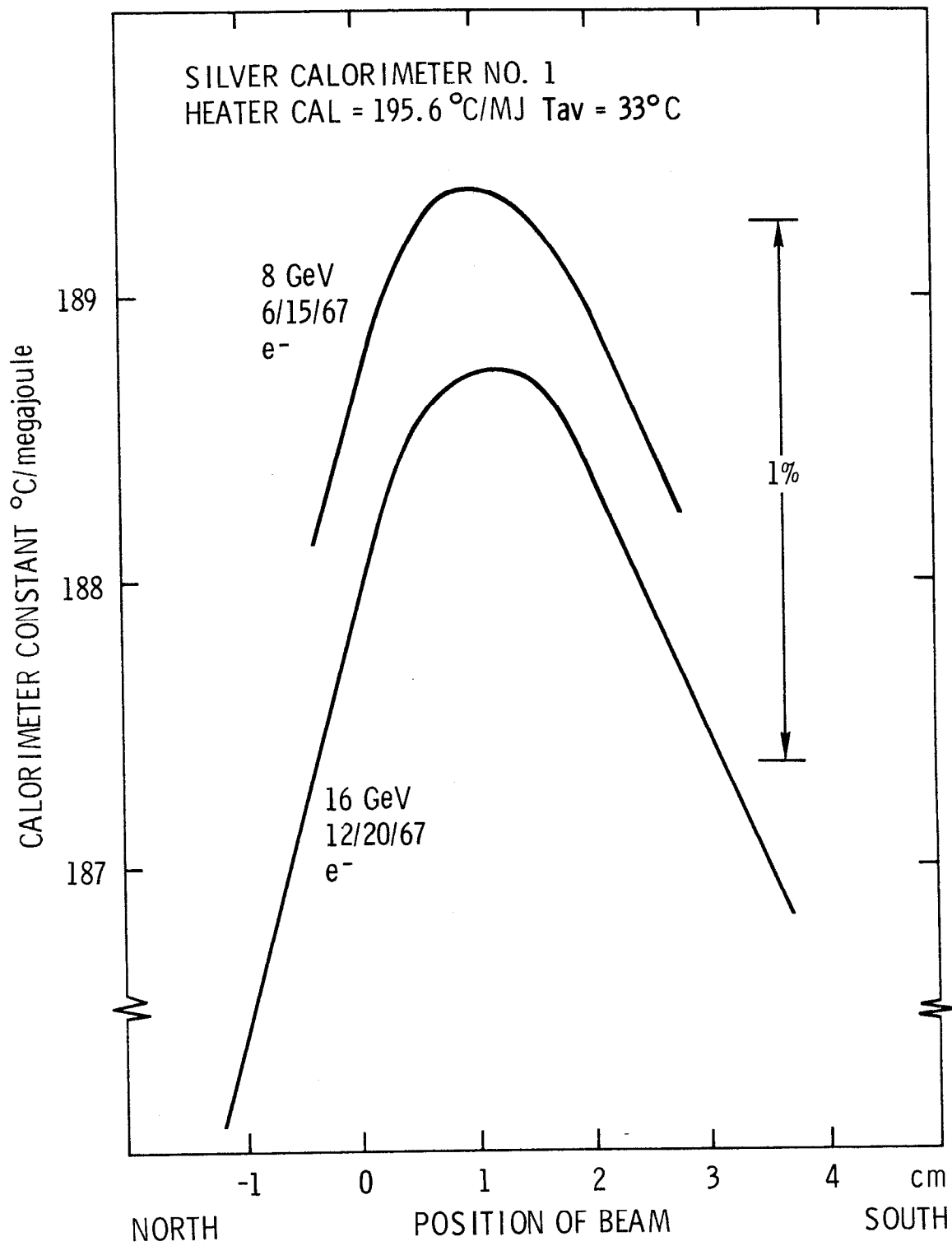
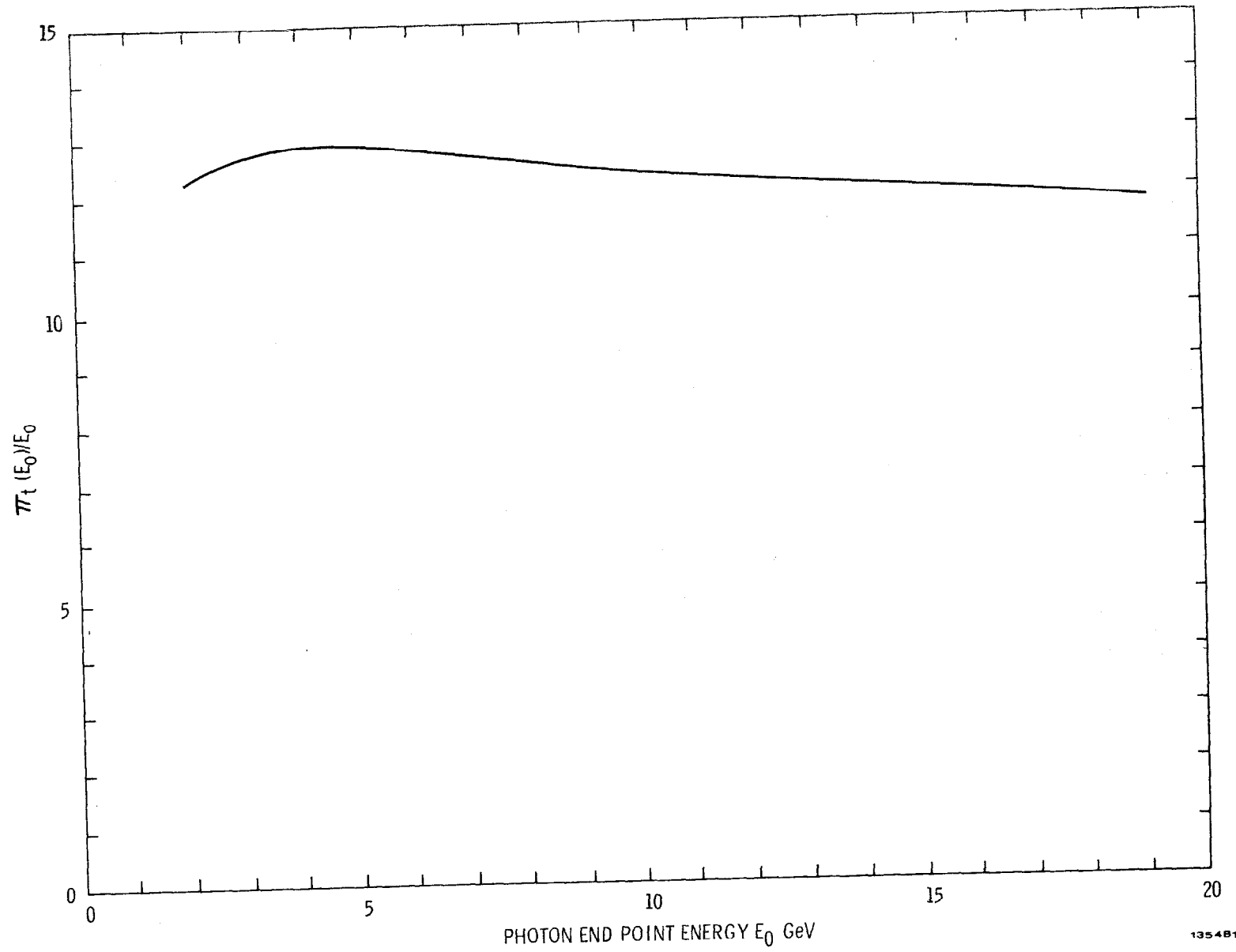


Fig. 9



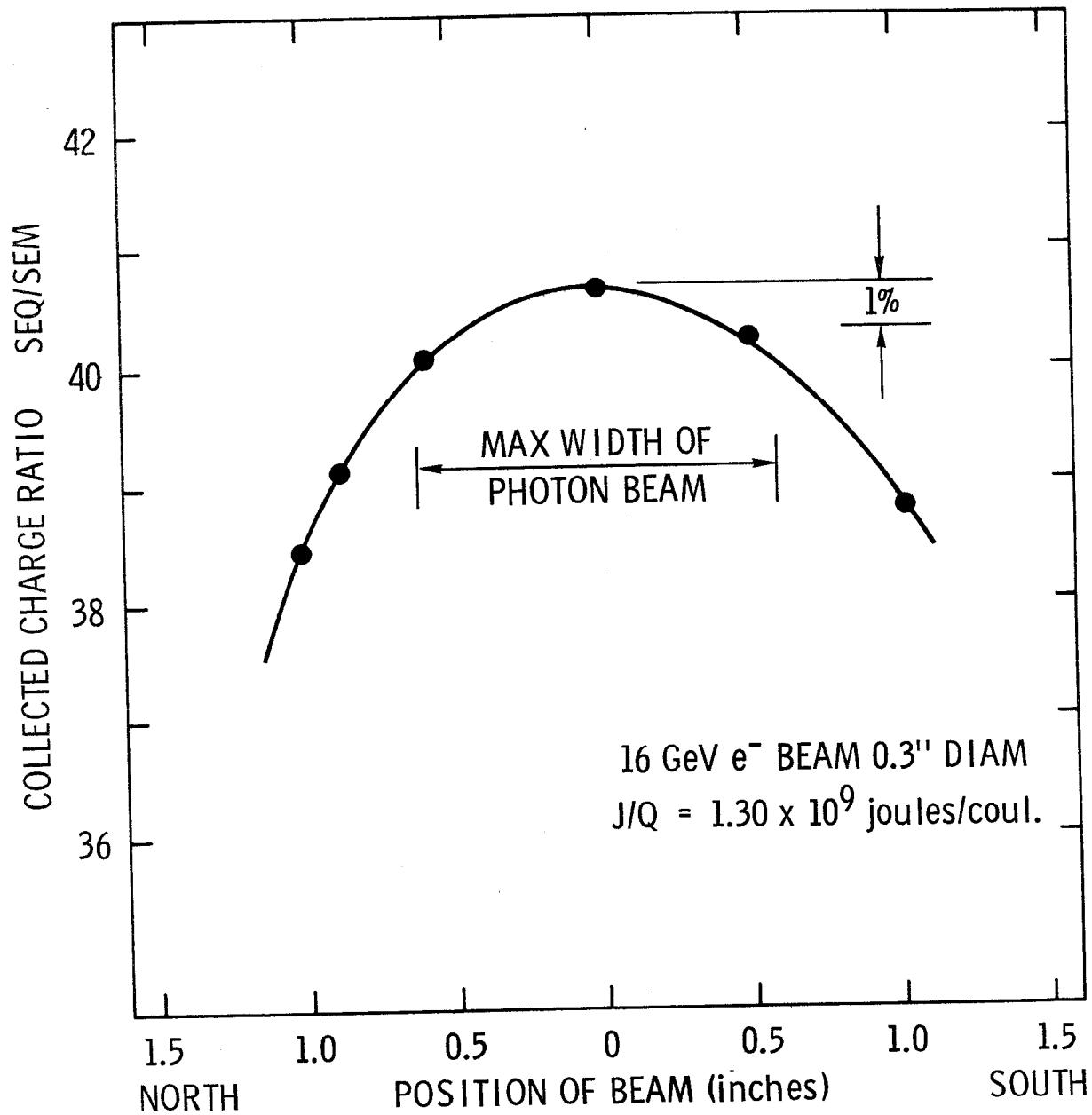
1354810

Fig. 10



1354811

Fig. 11



1354A12

Fig. 12

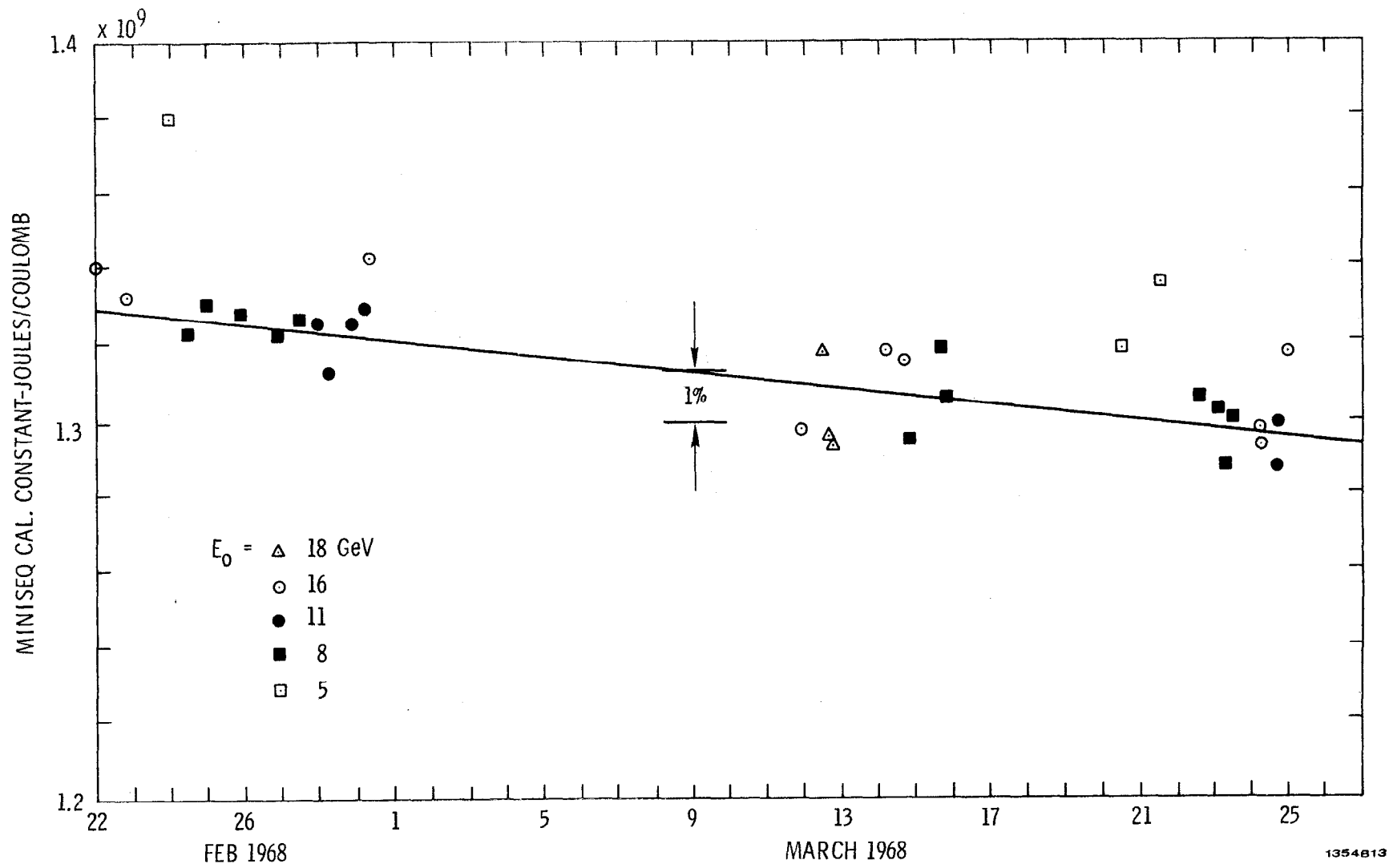
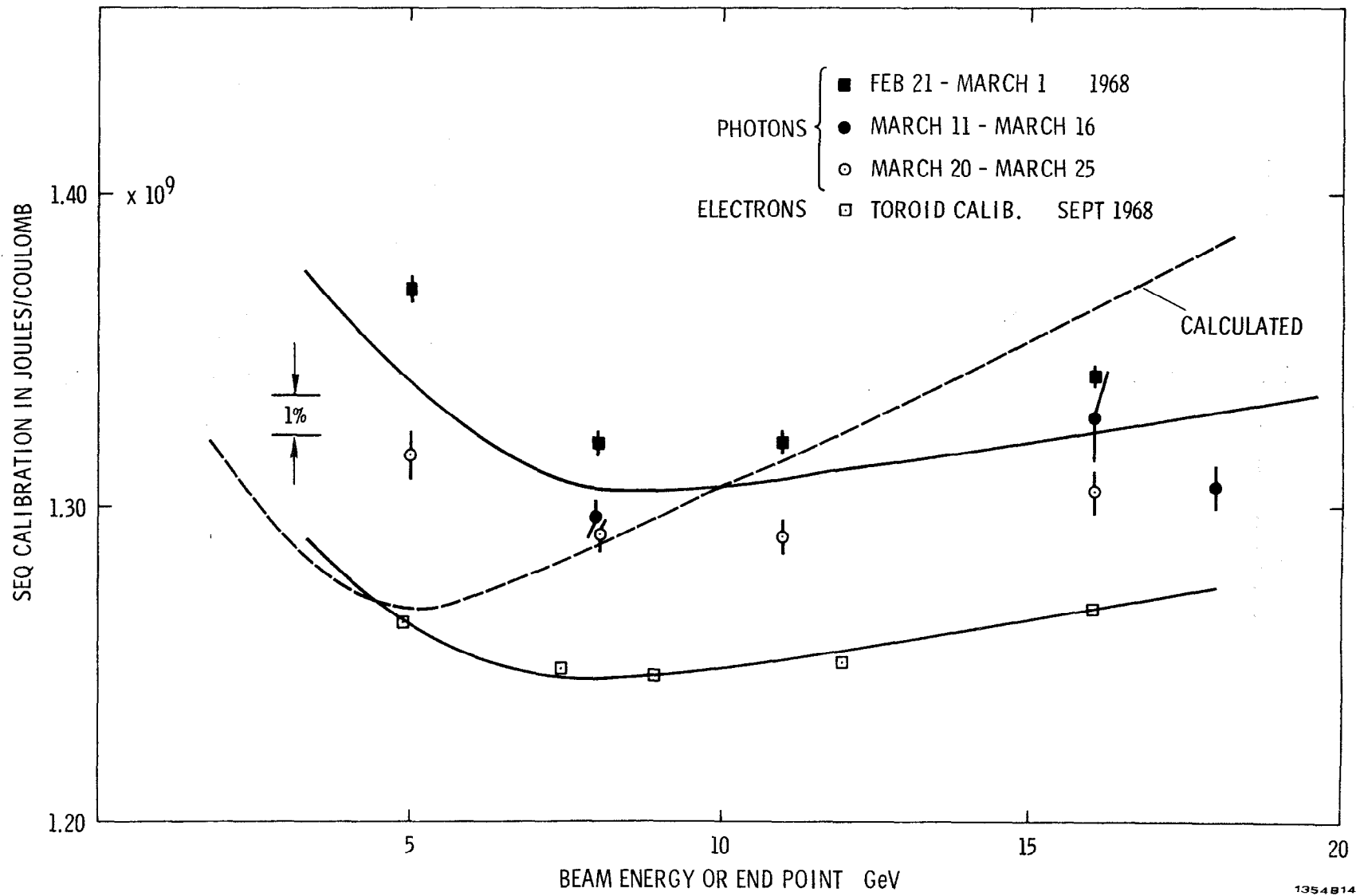


Fig. 13



1354B14

Fig. 14

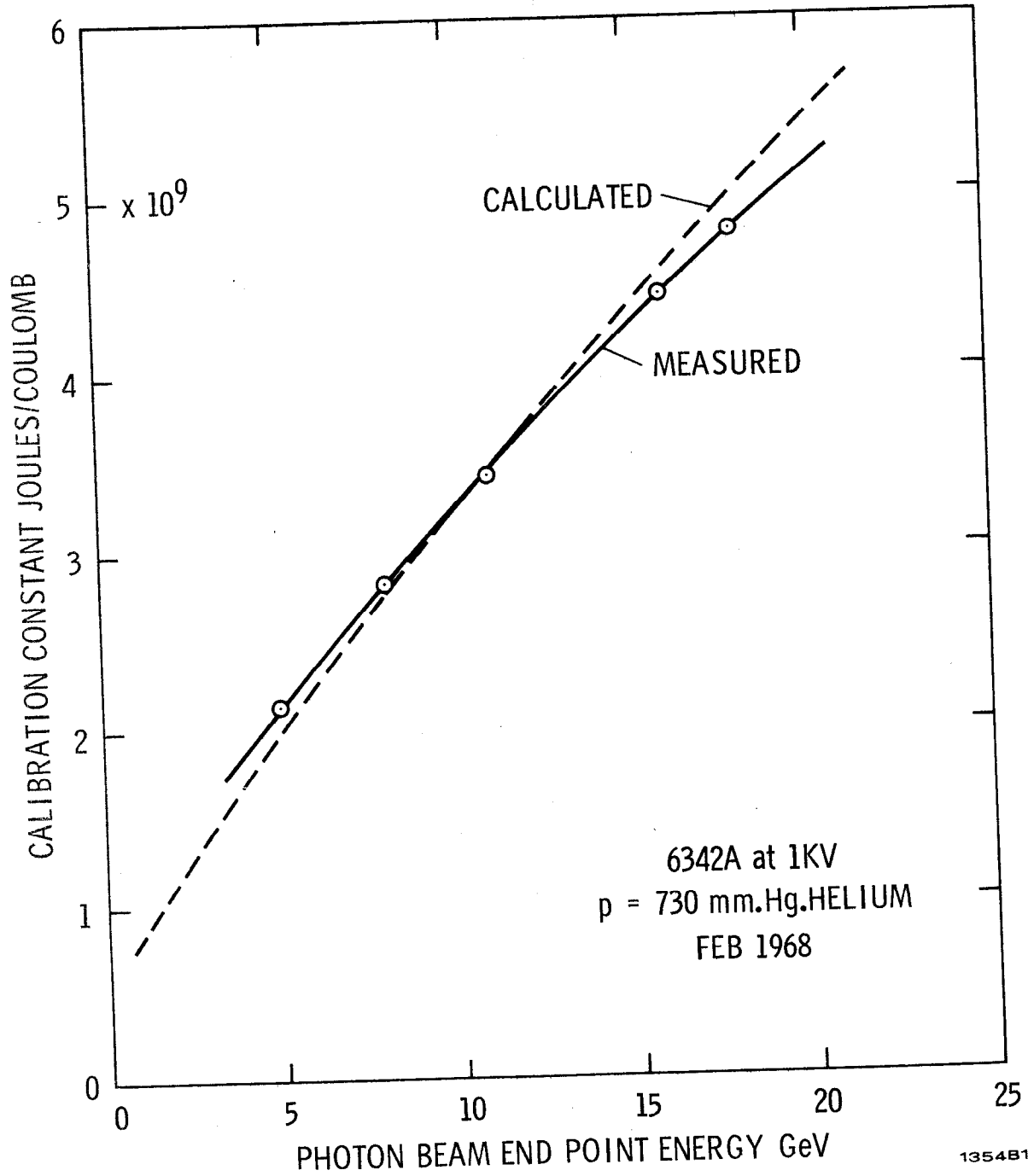


Fig. 15